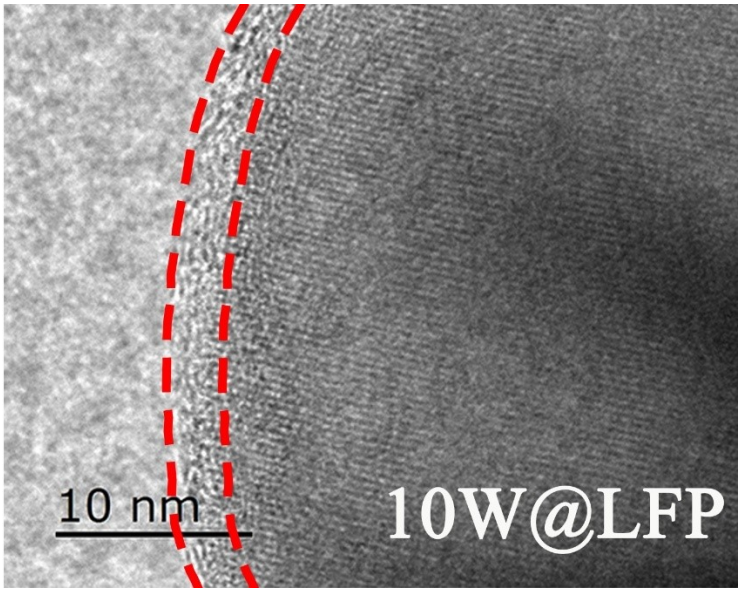

Fig. S1 TEM image of 10W@LFP sample.

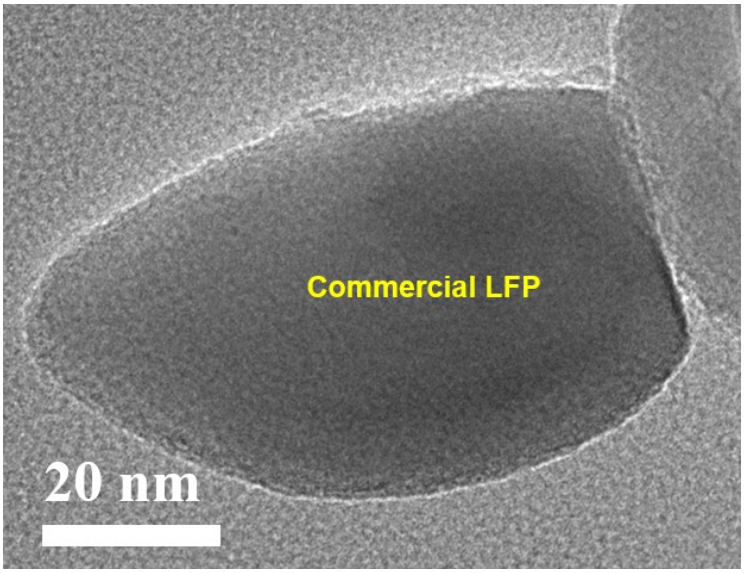

Fig. S2 TEM image of the commercial LFP.

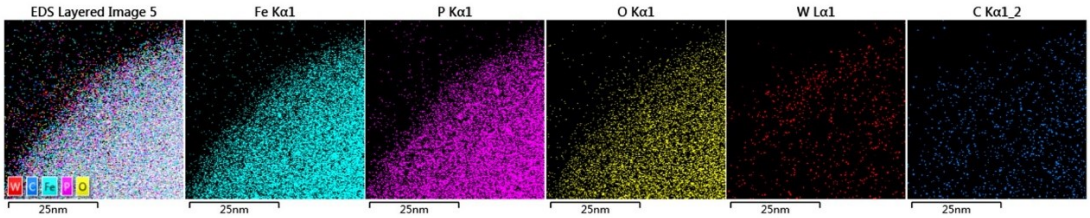

Fig. S3 TEM EDS mapping images of the 10W@LFP.

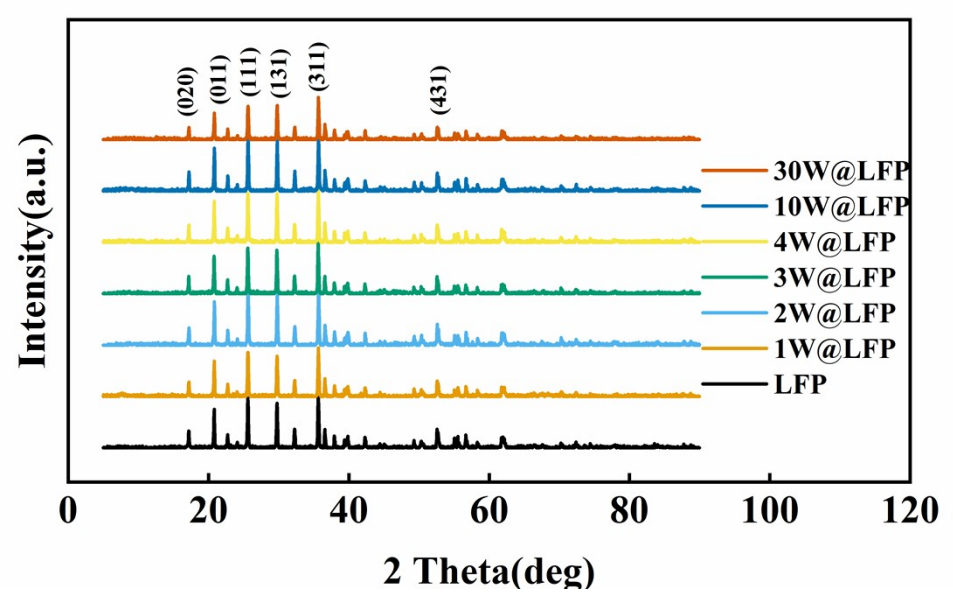

Fig. S4 XRD patterns of the coated with different numbers of W ALD cycles (x = 0, 1, 2, 3, 4, 10, 30).

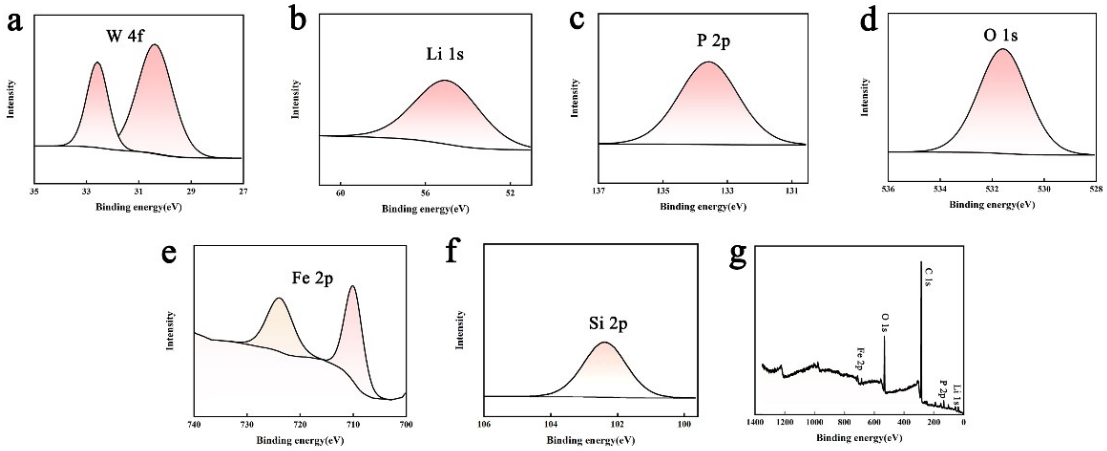

Fig. S5 XPS survey spectrum of the 2W@LFP sample.

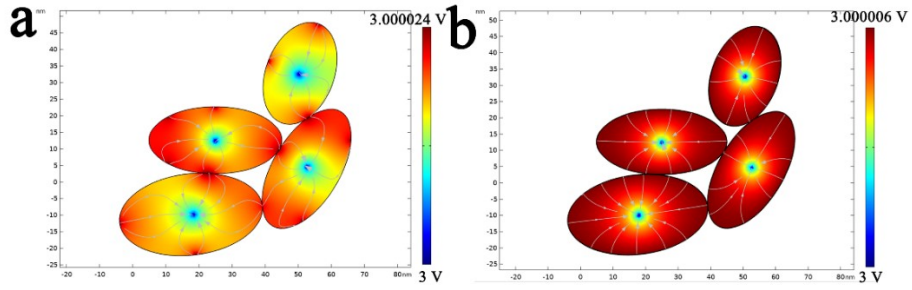

Fig. S6 COMSOL simulation illustrating the proposed mechanism of enhanced conductivity: (a) the LFP and (b) the 2W@LFP.

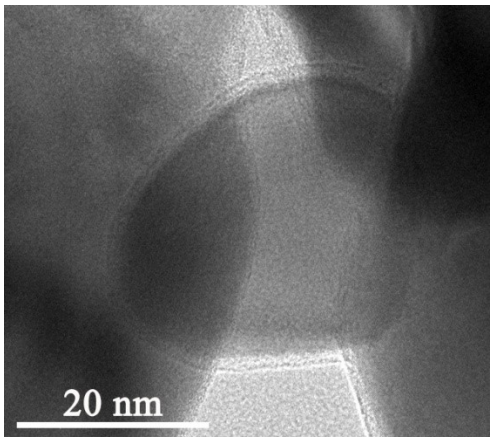

Fig. S7 Uniform W coating is observed on the surface of primary LFP particles.

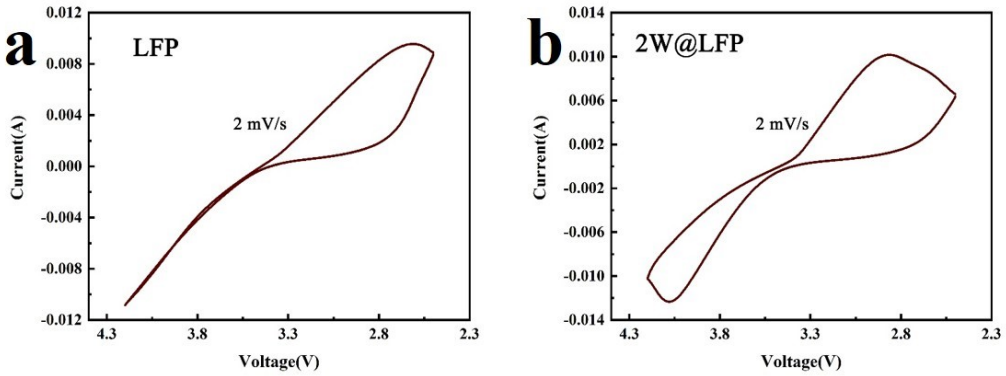

Fig. S8 CV curves of (a) LFP and (b) 2W@LFP at a scan rate of 2 mV s^{-1}.

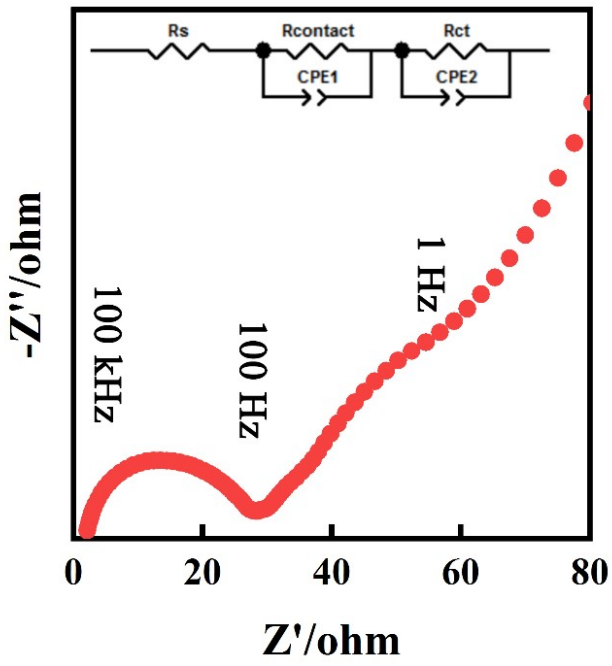

Fig. S9 Electrode-level EIS fitting and Equivalent circuit model used for impedance analysis

of 2W@LFP sample.

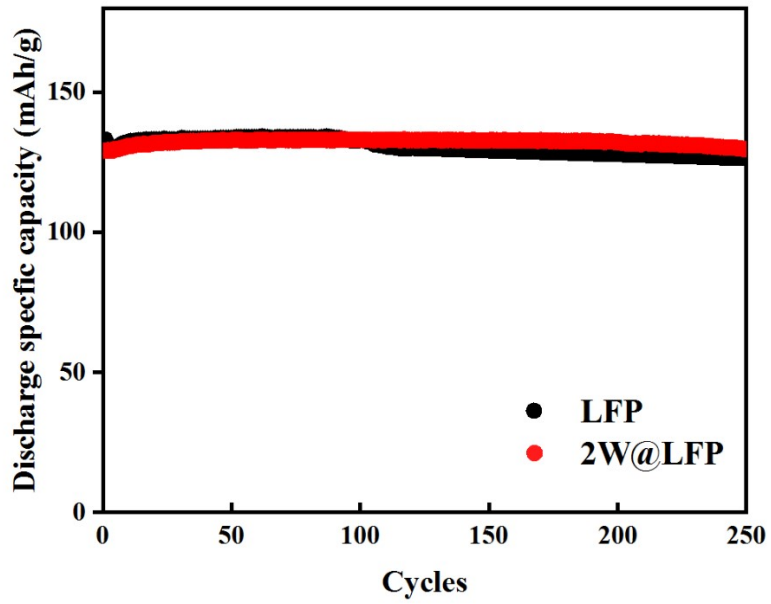

Fig. S10 Cycling performance of LFP and 2W@LFP samples at 3C.

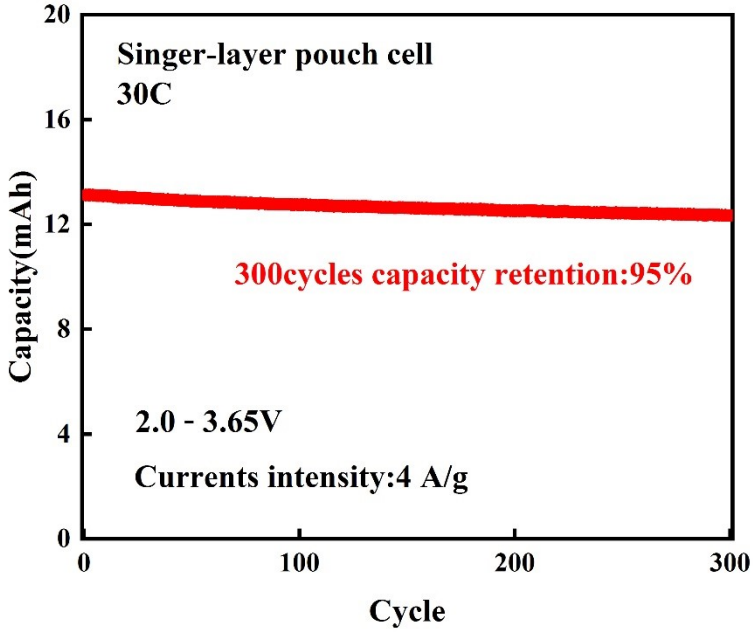

Fig. S11 Cycling performance of the 2W@LFP at 4A g^{-1}.

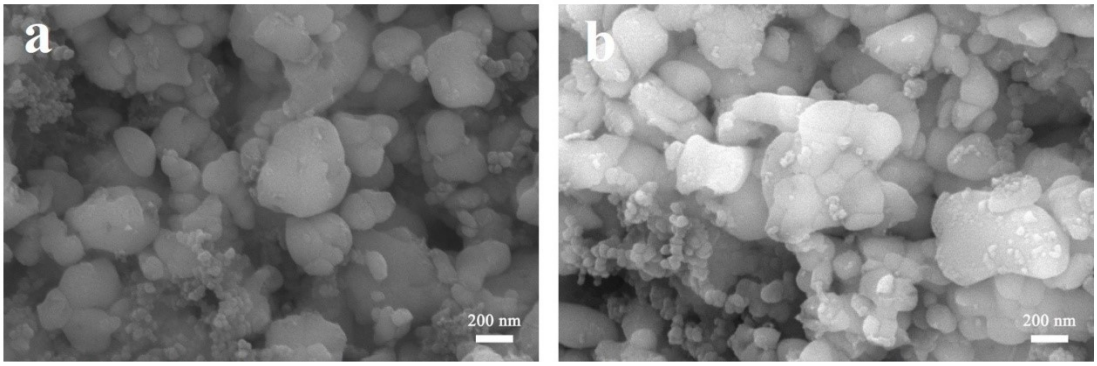

Fig. S12 SEM images of (a) the LFP and (b) the 2W@LFP electrodes.

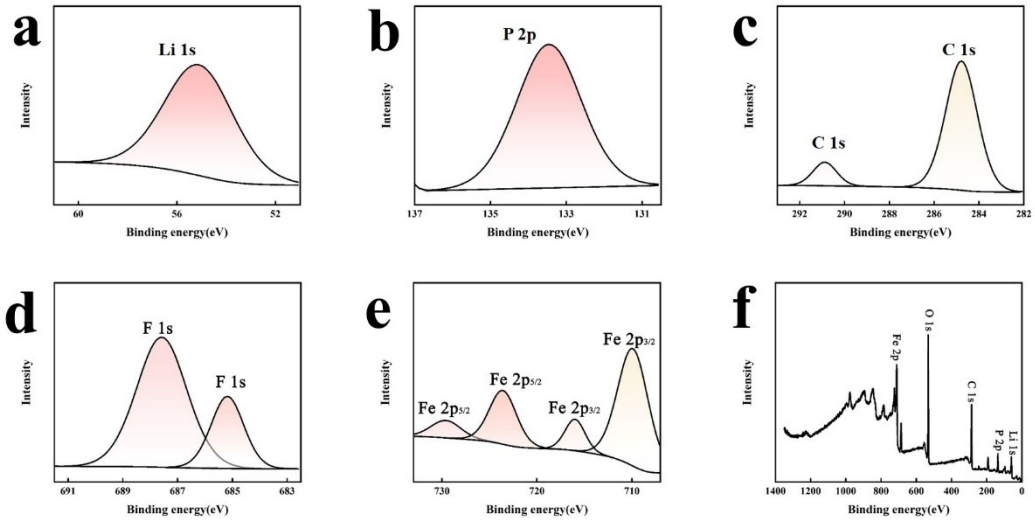

Fig. S13 XPS survey spectrum of the LFP electrode after 300 cycles.

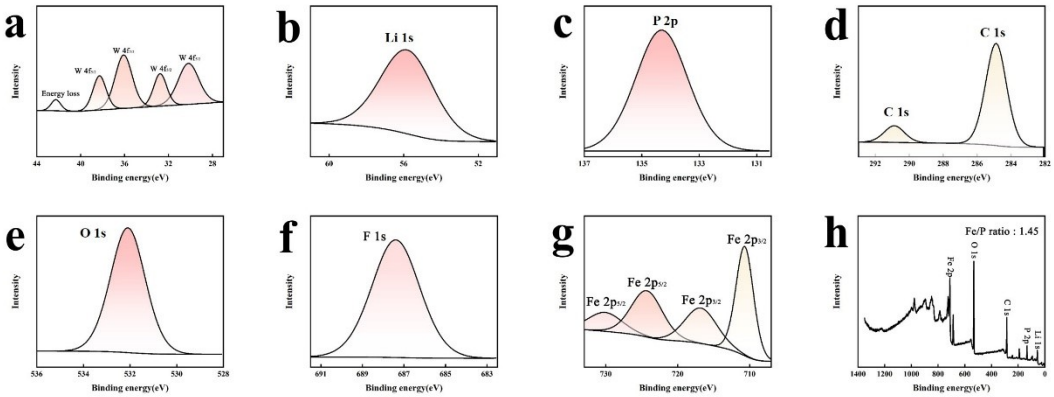

Fig. S14 XPS survey spectrum of the 2W@LFP electrode after 300 cycles.

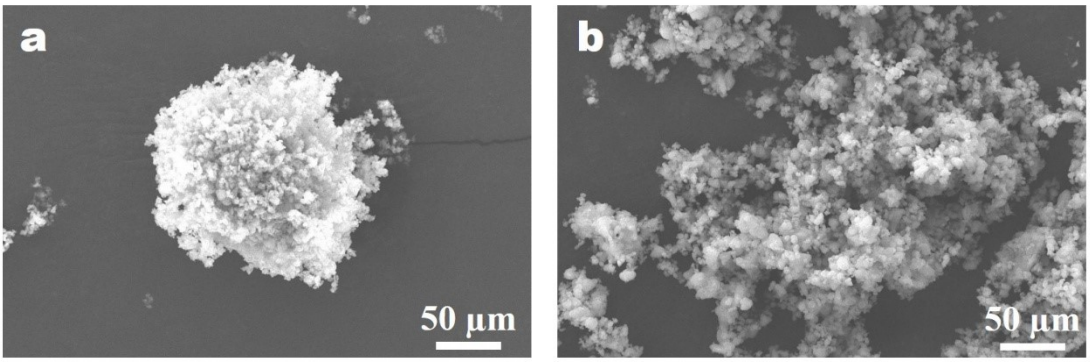

Fig. S15 SEM images of (a) the LFP and (b) the LFP-d3.

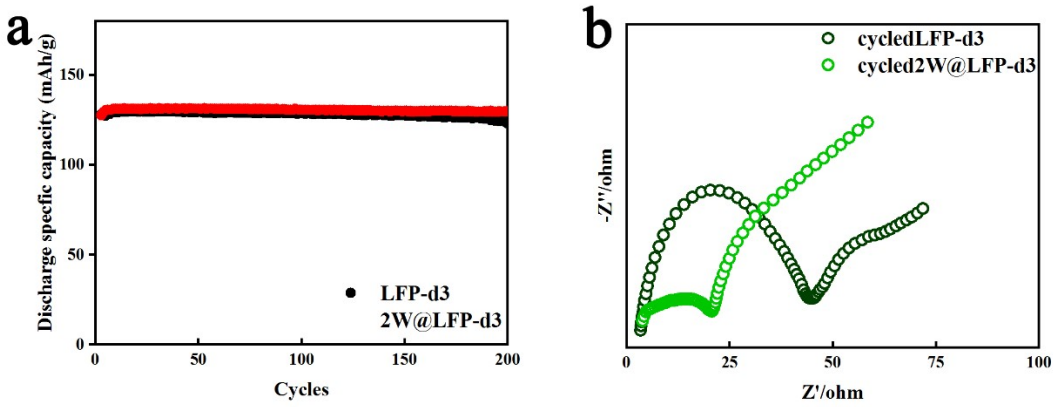

Fig. S16 Cycling retention of LFP-d3 and 2W@LFP samples.

Tab S1 Carbon-free conductive coating methods on $LiFePO_4$ material.

Coating	Method	5C capacity	Max rate	Refs
Ni and Cu	corecipitation	117 mAh/g	5C, 117 mAh/g	Journal of Physics and Chemistry of Solids, 2026, 208, 113150
Ag	solution	94 mAh/g	5C, 94 mAh/g	Electrochimica Acta, 2018, 265, 160
Al_2O_3	ALD	-	1C, 120 mAh/g	ECS Meeting, 2022, 306
TiN	ALD	83 mAh/g	10C, 48 mAh/g	Journal of the Electrochemical Society, 2018, 165, 3871
W	ALD	132 mAh/g	30C, 113 mAh/g	This work

Note. S1:

The powder was uniaxially cold-pressed into pellets (10 mm diameter) at a pressure of 25 MPa for 5 minutes using a standard hydraulic press. All LFP and W@LFP powder samples were prepared under identical conditions, including the same sample mass (100 mg), the same mold diameter (10 mm), the same pressing pressure (25 MPa), and the same holding time (5 min).

Note. S2:

Based on the COMSOL platform, the electronic conduction behavior of LFP particles before and after tungsten coating was computationally investigated. Due to the prohibitive computational cost and mesh generation difficulty for a full micron-sized LFP particle with a 0.6 nm coating, we performed finite element simulation using 20 nm primary LFP particles, on which a uniform W coating is confirmed by TEM (Fig. S7 in the Supporting Information). The key physical picture that electrons preferentially conduct along the low-resistance surface coating is valid for both the 20 nm primary particles and the 6 μm secondary particles.

In the simulations, several 20 nm LFP grains were modeled, with a coating thickness of 0.6 nm for the W coating group. The finite element models were discretized using a free triangular mesh to ensure simulation accuracy. In this model, the conductive carbon black and PVDF binder within the LFP electrode form a network that connects to the LFP grains only at discrete point contacts. During charge and discharge, electrons are transported through these contact points. When the LFP electrode is operated near its rate capability limit, its low intrinsic electronic conductivity leads to a significant potential gradient.

The internal potential difference across a single LFP particle was estimated using Ohm's law in the form $J=\sigma\cdot\nabla V$, where J is the current density, σ the electronic conductivity, and ∇V the potential gradient. The current density was obtained from the macroscopic electrode current I divided by the geometric area A of the cathode pellet in a coin cell ($A \approx 0.5$ cm^2). At a discharge rate of 10 C, the measured current was in the range I = 2.2 mA to 2.5 mA. Using the average value I = 2.35 mA, thus J =I / A = 4.7 e^{-3} A/cm^2. The electronic conductivity of LFP sample is σ_{LFP} = 4.07e^{-4} S/cm, while that of 2W@LFP sample is $\sigma_{2W@LFP}$ = 1.52e^{-3} S/cm. The potential gradients are then $\nabla V_{LFP} = J / \sigma_{LFP}$ = 12 V/cm, $\nabla V_{2W@LFP} = J / \sigma_{2W@LFP}$ = 3 V/cm. Multiplying these gradients by the particle diameter d = 20 nm = 20e^{-7} cm yields the voltage difference across one particle: $\Delta V_{LFP} = \nabla V_{LFP}$ * 20 nm = 0.024 mV, $\Delta V_{2W@LFP} = \nabla V_{2W@LFP}$ * 20 nm = 0.006 mV.

Note. S3:

The Li^+ diffusion coefficient (D_{Li+}) was calculated from the low-frequency region of the EIS spectra using the following equation:

$$D_{Li+}=1/2*R^2T^2*A^2n^4F^4C_0^2\sigma^2$$

where R is the gas constant (8.314 J mol^{-1} K^{-1}), T is the absolute temperature (298 K), A is the surface area of the electrode (1.54 cm^2), n is the number of electrons transferred per reaction (n = 1 for LFP), F is the Faraday constant (96485 C mol^{-1}), C_0 is the concentration of Li^+ in the electrode (7.69 × 10^{-3} mol cm^{-3}), and σ is the Warburg coefficient obtained from the slope of the linear fit of Z' vs. $\omega^{-1/2}$ (as shown in the inset of Fig. 3d). The calculated σ values for LFP and 2W@LFP are 282 and 140 Ω s$^{-1/2}$, respectively. Consequently, the D_{Li+} values for

LFP and 2W@LFP are calculated to be 5.8×10^{-13} and 2.61×10^{-12} $cm^2\ s^{-1}$, respectively.